Multiple attenuation using a high-resolution time-domain Radon transform

Zhihong Cao and John C. Bancroft

ABSTRACT

A high-resolution time-domain Radon transform is used to identify and separate multiple energy from seismic reflection energy. The transform used is an optimized semblance-weighted Radon transform. In this method, the highest energy trajectories are identified first in the Radon domain, then the energy is subtracted immediately from the source gather before it is used by other trajectories. This process improves the spatial resolution of the energy in the Radon domain.

The high-resolution time-domain Radon transform was applied to real and synthetic data and produced encouraging results.

INTRODUCTION

The Radon transform has been an industry standard on multiple attenuation in seismology for decades. Geophysicists have been investigating the Radon transform for a number of decades to improve the resolution of the algorithm so that a better separation between primaries and multiples can be achieved when the algorithm is applied to seismology.

The theory of the Radon transform has been previously reviewed and discussed by the authors (Cao and Bancroft, 2003, 2004 and 2005). The concept is briefly introduced here. The forward parabolic transform is defined as (Radon, 1917; Yilmaz, 1989):

$$u(\tau, q) = \sum_x d\left(t = \tau + qx^2, x\right), \tag{1}$$

where $d(t, x)$ represents a seismic dataset in time-space domain such as a CMP gather; $u(\tau, q)$ represents a dataset in the Radon domain; x is a spatial variable, such as offset; q is the slope of the curvature; τ is the intercept time; and t is the two-way traveltime. The logical inverse Radon transform is defined as:

$$d'(t, x) = \sum_q u\left(\tau = t - qx^2, q\right), \tag{2}$$

where $d'(t, x)$ is the reconstructed dataset in the time-space domain from the Radon domain. A major problem of the forward Radon transform is smearing, that is described by a model in Figure 1 (a) and its Radon panel computed by Equation (1) in Figure 1 (b). A parabolic event in Figure 1 (a) is transformed into a smeared event in Figure 1 (b) in stead of a focused point, which the optimized semblance-weighted Radon transform or the high-resolution time-domain Radon transform strives to achieve.

The optimized semblance-weighted Radon method is based on the semblance-weighted method. Both of the methods are introduced in this report.

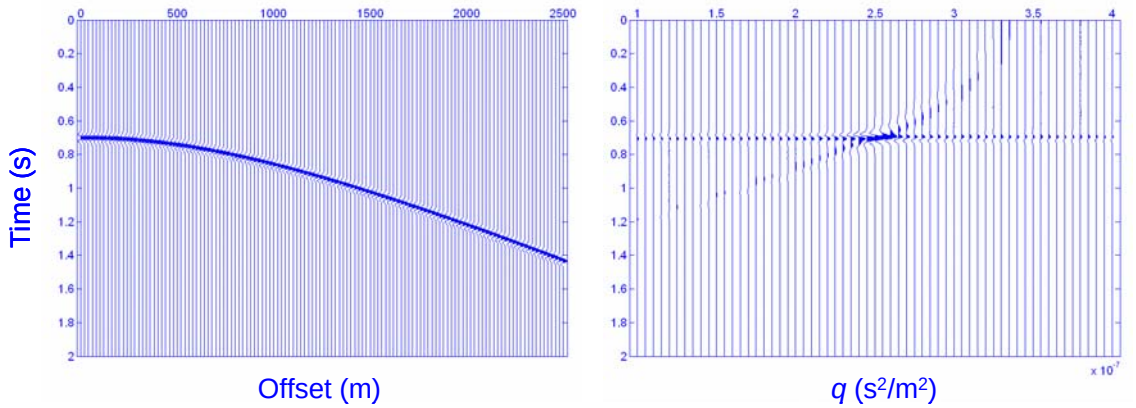

FIG. 1. A CMP gather and its Radon panel calculated by the conventional Radon transform

SEMBLANCE-WEIGHTED RADON TRANSFORM

Bradshaw and Ng (1987, unpublished) worked on the parabolic semblance-weighted Radon transform with the Gauss-Seidel iterative method in the time domain. The weight function, semblance, defined by Stoffa et al. (1981), can be written as follows along parabolic trajectories:

$$S(\tau,q)=\frac{\sum_{l}\left(\sum_{x} d\left(t=\tau+qx^2,x\right)\right)^2}{N_x\sum_{l}\sum_{x} d^2\left(t=\tau+qx^2,x\right)}, \tag{3}$$

where l is a window size, and N_x is the number of traces in the time-space domain involved in the semblance calculation. Semblance has an important property that its value is only dependent on the coherency of events and independent of the amplitudes of the input dataset; it ranges from 0 to 1, indicating poorest to best fit of the proposed trajectory respectively (Bradshaw and Ng, 1987). Weighting the forward Radon transform with semblance can enhance energy cluster along those trajectories which fit seismic events well in the seismic dataset while attenuating energy along those trajectories which badly fit seismic events. Applied in the Gauss-Seidel sense, the semblance-weighted Radon approach produces moderately high-resolution results. The weighted parabolic Radon transform is then defined as follows:

$$u(\tau,q)=S(\tau,q)\sum_{x} d\left(t=\tau+qx^2,x\right). \tag{4}$$

The semblance plot of the model in Figure 1 (a) is shown in Figure 2 and its Radon panel computed by Equation (3) is shown in Figure 3. Comparing the Radon panels in Figure 1(b) and Figure 3, the latter gives more focused energy in the Radon domain.

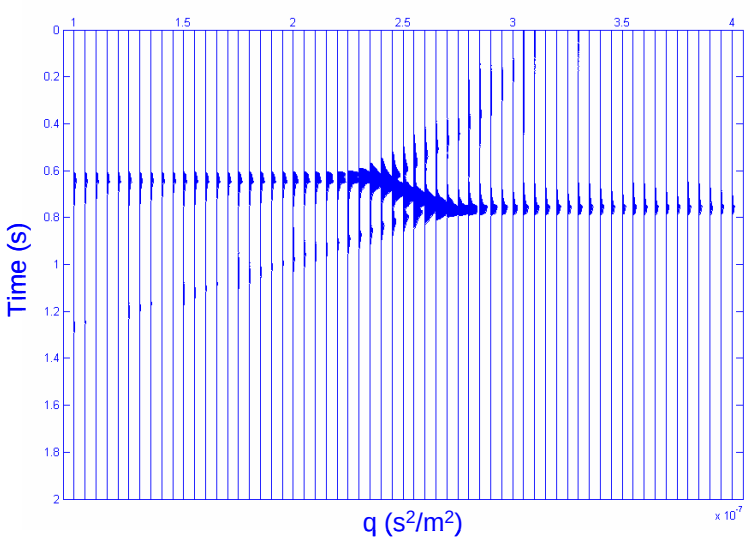

FIG. 2. The semblance plot of the model in Figure 1 (a).

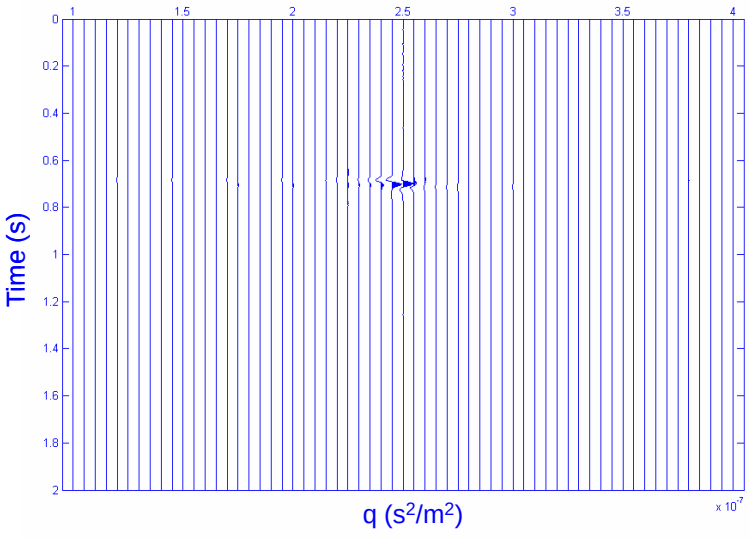

FIG. 3. The Radon panel of the model in Figure 1 obtained by the semblance-weighted Radon solution (scaled to Figure 1 (b)).

THE HIGH-RESOLUTION RADON TRANSFORM

A high-resolution time domain Radon solution or an optimized semblance-weighted Radon solution using the Gauss-Seidel scheme was proposed by Ng and Perz (2004). In order to utilize the previous transform computed by the semblance-weighted Radon method introduced above as a priori information in the current transform to achieve sparseness in a Gauss-Seidel scheme, a well-known property of the Gauss-Seidel algorithm should be discussed. For early iterations in the Gauss-Seidel algorithm, the model energy tends to reside in whichever model components are estimated first. The

Gauss-Seidel calculation of the semblance-weighted method is based on a sequential q index, which leads to energy preference to those q traces which are estimated first. The results from the semblance-weighted method are then used to estimate the power of q and a new sequence of q traces is generated. A new process of semblance-weighted Radon transform now starts over using the current q-estimation sequence. The initial input gather is still the original t-x CMP gather. This scheme ensures that the most significant q traces are estimated first and contain the strongest energy, which leads to a solution sparse in the q direction. Optionally, the current transform becomes the new preliminary results for a revised q-estimation sequence and the process is repeated.

The procedure of the Gauss-Seidel iterations of the optimized semblance-weighted Radon solution is summarized as follows:

(a) Calculate the Radon panel, $\mathbf{u}_1$, of the input gather $\mathbf{d}_k$ using the semblance-weighted Radon method .

(b) Sort the q sequence based on energy cluster of $\mathbf{u}_1$.

(c) Start from q_i=q_1, then increment to q_2, q_3, … according to the q sequence obtained in step (b), to stack the input gather $\mathbf{d}_k$ (k is the iteration number and the initial input is the original dataset $\mathbf{d}$) along the proposed trajectory q_i; calculate the semblance of the gather along this trajectory; weight the stack with the semblance. This gives an estimate $u_{est}(\tau, q_i)$ at this q_i trace.

(d) Compute the inverse Radon transform $\mathbf{d}_k^{'}$ at this q_i trace and subtract it from the current input gather to create a new dataset $\mathbf{d}_{k+1}$, which is called residual gather and will be the new input dataset to calculate the Radon transform along the next trajectory q_{i+1}. The input energy gradually diminishes as the calculation proceeds and the Gauss-Seidel iterations increase.

(e) Add the current estimate at q_i trace, $u_{est}(\tau, q_i)$, to the accumulated estimate in the transform domain, $u_{acc}(\tau, q_i)$.

(f) Increment to the next q trace, q_{i+1}, based on the q sequence and repeat steps (c) to (e) until all q traces are covered. The only difference is that the input dataset in step (c) will now be the residual dataset $\mathbf{d}_{k+1}$ obtained in step (b).

In order to demonstrate the algorithm strategy that the optimized semblance-weighted Radon transform adopts, a model is shown in Figure 4. with its 5 tentative Radon transform stacking trajectories, from top to down, with corresponding to Trace 1, 2, 3, 4 and 5 respectively in Figure 5, which shows an enlarged portion of the Radon panel of the model. The true velocity of the event corresponds to Trace 3, which stands for a perfect fit trajectory of the event in Figure 4. Once the initial Radon model, Figure 5, is obtained by the semblance-weighted Radon transform, the energy along the q-axis can be

estimated, which is indicated in Figure 5 by a trapezoid. Apparently, Trace 3 has the highest energy accumulation among all the traces.

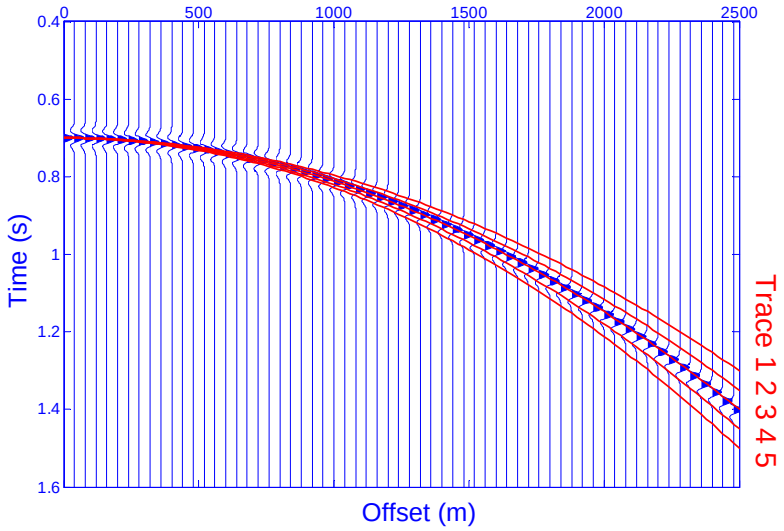

FIG. 4. A model with 5 tentative stacking trajectories.

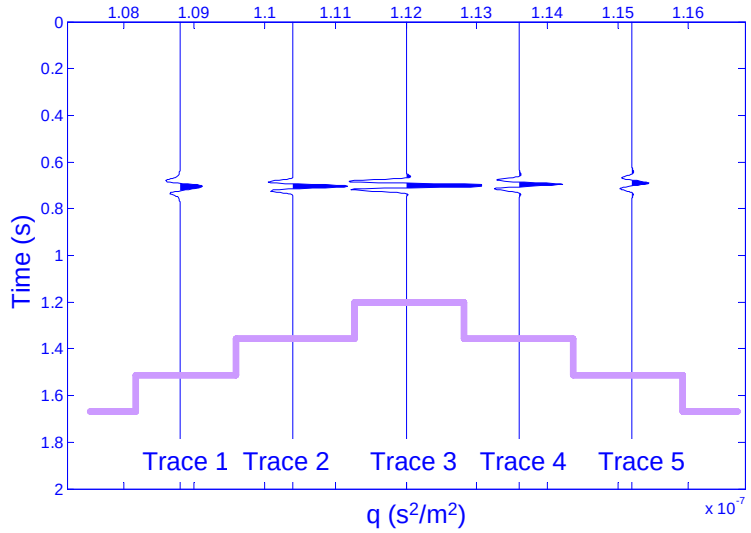

FIG. 5. A small portion of the Radon transform of the model in Figure 4..

The second iteration of the optimized semblance-weighted algorithm will be first employed over Trace 3 and the Radon panel obtained is shown in Figure 6. The data which are already transformed into the Radon space are then removed from the input gather, and the residual gather, shown in Figure 7, will be the new input data for the next *q* trace, which in this case could be Trace 2 or 4.

Since the trajectory of Trace 3 is an ideal fit of the event, there is not much energy left after the first run over Trace 3. When we move to the next *q* trace, there is not much smearing energy that can be brought in (Figure 8).

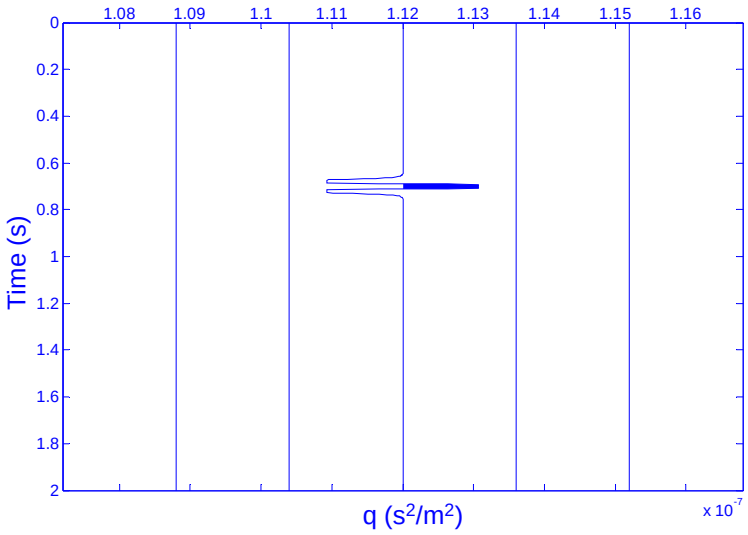

FIG. 6. The Radon panel of the model obtained by working on Trace 3.

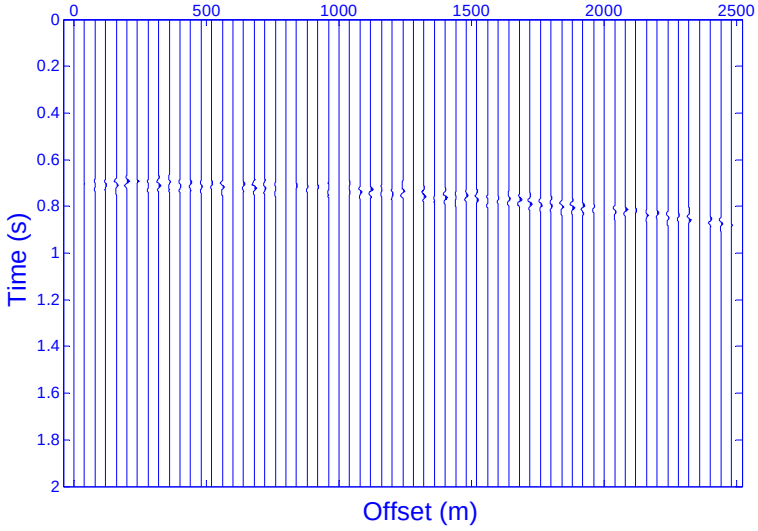

FIG. 7. The updated input data after the data along Trace 3 that have been transformed into the Radon space are removed from the original input data.

DATA EXAMPLES

Synthetic data examples

A synthetic NMO-corrected CMP gather shown in Figure 9. contains offsets from 0 to 2500 m and the trace interval is 20 m. Two primaries, Pa and Pb, with constant amplitudes across the offsets, flat after NMO correction, are located at 0.3 s and 0.57 s respectively. One of the five multiple events in parabolic shapes, Ma, has the same traveltime as Pa at zero offset and its moveout at the far offset is 20 ms. Notice from Figure 10., an enlarged portion of Figure 9., that Ma is very close to Pa and they are difficult to differentiate. They are partially mixed with each other even at far offsets and there is only 20 ms between their peaks at the farthest offset. Mb, with a zero offset

traveltime of 0.5 s and moveout of 70 ms at the far offset, overlaps the primary Pb at far offsets. The event

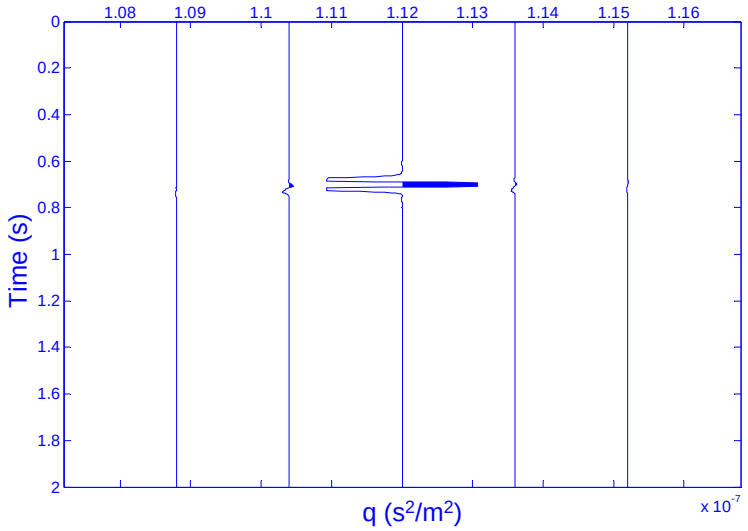

FIG. 8. The final Radon panel of the model in Figure 4. by the optimized semblance-weighted Radon solution.

Mc is located at 0.7 s at zero offset. This event has uniform amplitudes and is not interfered with by any other event. Md, with a vertical traveltime of 1.02 s and a moveout of 120 ms at the far offset, has variable amplitudes at the near offsets; and Me, with a vertical traveltime of 1.3 s and a moveout of 150 ms at the far offset, shows variable amplitude effects at far offsets.

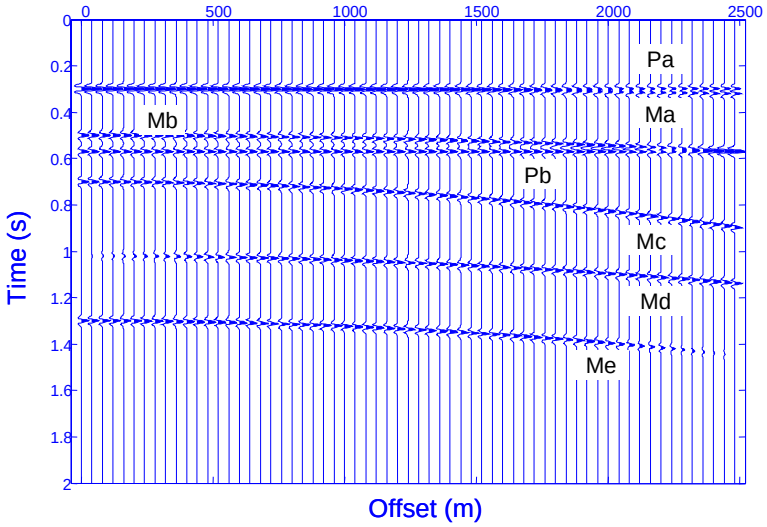

FIG. 9. A synthetic NMO-corrected CMP gather including two primaries Pa and Pb and five multiples Ma, Mb, Mc, Md and Me.

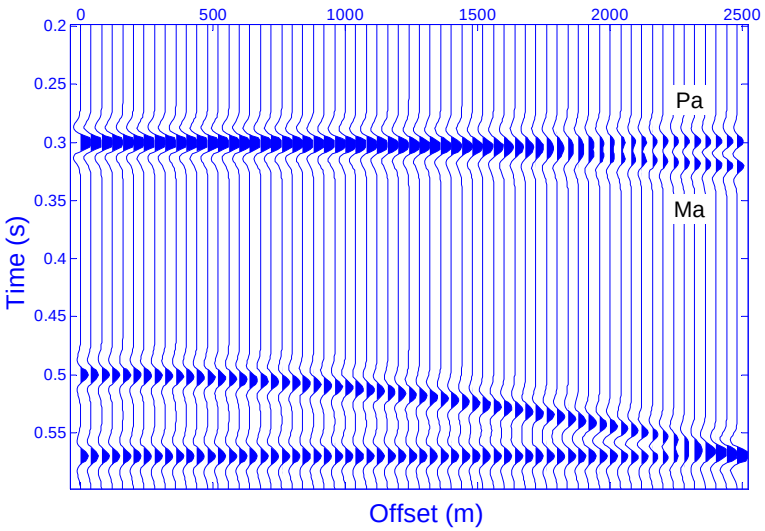

FIG. 10. An enlarged portion of the model in Figure 9. Notice that Pa and Ma are hard to separate even though they are enlarged.

The results of the Gauss-Seidel iterative semblance-weighted Radon method introduced by Bradshaw and Ng (1987) are shown in Figure 11. The utilization of semblance information defined by Equation (3) in the weighting function of the Radon transform, Equation (4), results in the sparsity constraints in the Radon panel as shown in Figure 11. (b). The Gauss-Seidel iterative method attempts to minimize the smearing problem by removing the transformed energy from the original input dataset for each q trace during calculation. However, the event Ma can not yet be separated from the event Pa even though this method resulted in fairly good resolution in the Radon panel. The reconstructed CMP gather shown in Figure 11. (c) and the residual energy in Figure 11. (d) show that reconstruction with minimal errors is obtainable by this method.

Even though Figure 11. (b) shows impressive results in the Radon panel, it is not yet optimum. The philosophy of the Gauss-Seidel method is that for early iterations, most of the energy in the data space, or in the CMP gather in this case, resides in whichever model components are estimated first (Ng and Perz, 2004). This is the reason why the Gauss-Seidel method still produces smearing energy in the Radon panel. During the implementation of the Gauss-Seidel algorithm, the calculation is performed based on sequential q traces. The high-resolution time domain Radon method strives to resolve this problem. The results of the improved Gauss-Seidel semblance-weighted Radon transform of the model in Figure 9. are shown in Figure 12. The Radon panel in Figure 12 (b) is impressive in that the events Pa and Ma can be clearly separated from each other even though there is only a 20 ms interval between the peaks of them at the farthest offset. The reconstruction of the CMP gather shown in (c) and the residual energy shown in (d) indicate very good data preservation.

It should be noted that these impressive result are obtained with ideal data to illustrate that capability of the process. Real data expectations may differ due to moveout stretch, noise, and imperfect moveout correction.

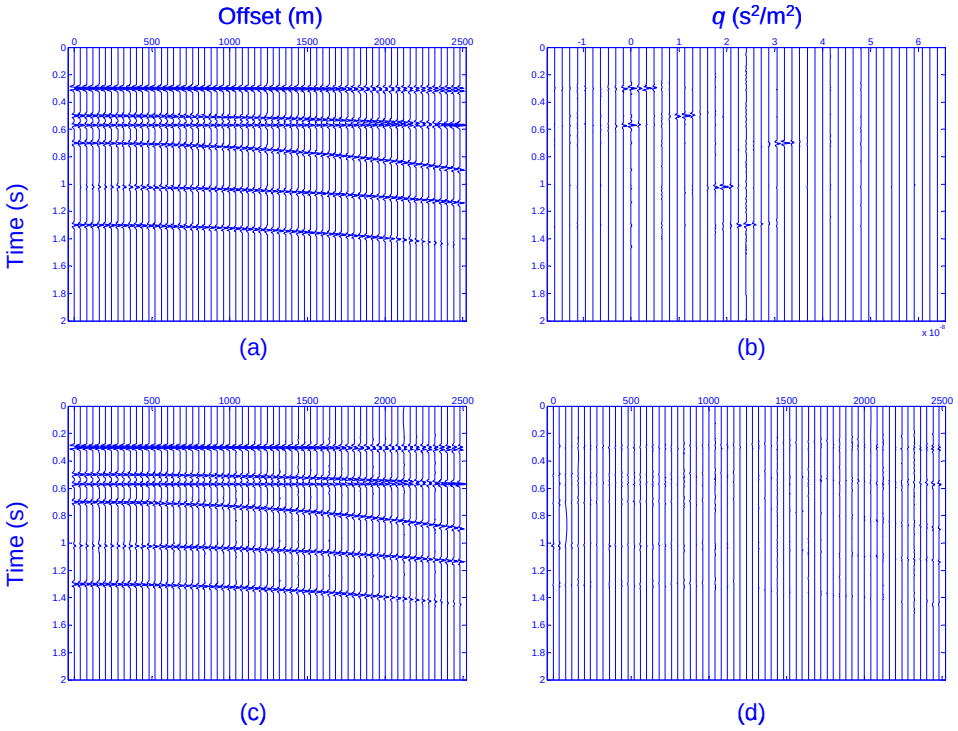

FIG. 11. Results of the semblance-weighted Radon method: (a) the model; (b) the Radon panel; (c) the reconstructed gather; and (d) the residual gather.

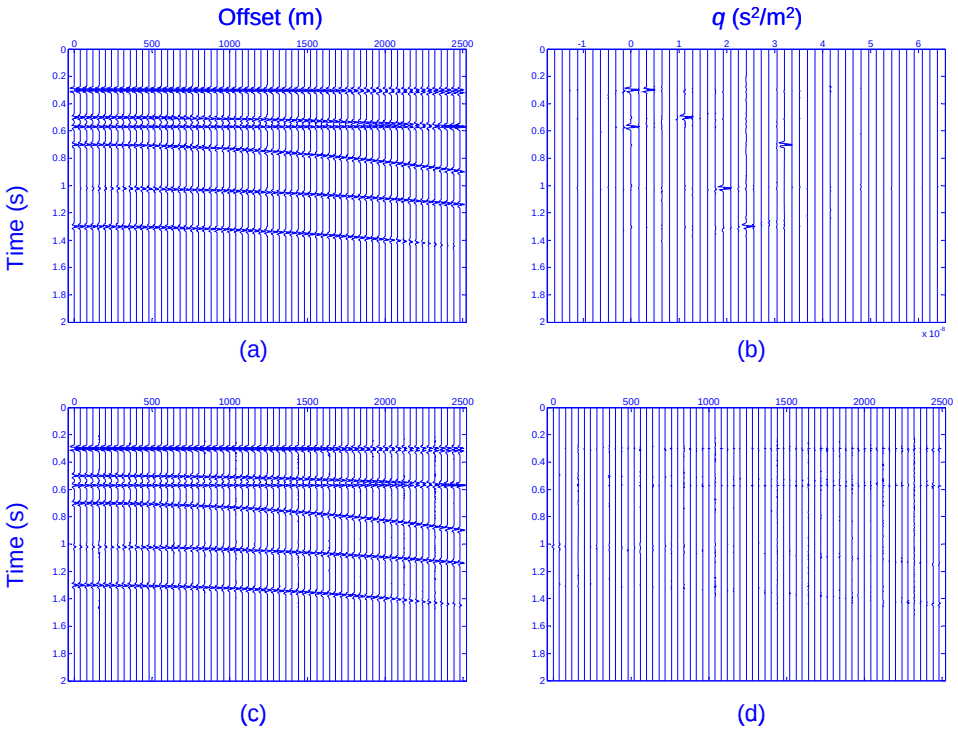

FIG. 12. Results of the optimized semblance-weighted Radon method: (a) the model; (b) the Radon panel; (c) the reconstructed gather; and (d) the residual gather.

Real data example

The White Rose oilfield is located offshore Newfoundland on the east coast of Canada. The water depth there is about 120 m. Due to the hard water-bottom, high ocean-bottom reflection coefficients create strong water-column reverberations in this area. High impedance contrast also occurs at the Tertiary-Cretaceous unconformity, which causes a serious peg-leg multiple problems. Underlying this Tertiary-Cretaceous unconformity is the target reservoir, the Avalon sandstone formation, which is strongly affected by the peg-leg multiples.

A CMP gather in this area shown in Figure 13 has been chosen to illustrate the serious multiple problems. From the figure, we can easily see the water-column reverberations above the reflection of the Tertiary-Cretaceous unconformity at about 2.2 s, and the peg-leg multiples of this reflector below 2.2 s with a periodicity of about 0.16 s. The strong multiples can also be recognized from the semblance plot of this CMP gather in Figure 14. The semblance plot also shows that there is a much weaker primary event located at about 2.7 s overlain by the strong peg-leg multiples of the Tertiary-Cretaceous unconformity. This reflection will be very hard to interpret on a stack section.

A faster computation of the Radon transform can be achieved by performing the algorithm on an NMO-corrected gather rather than an original gather since the NMO-corrected gather has a smaller range of moveout. The NMO-corrected version of the CMP gather in Figure 13 is shown in Figure 15 based on the velocity analysis in Figure 14. This NMO-corrected gather is used as the input for the optimized semblance-weighted Radon method and the obtained Radon panel is shown in Figure 16. The full reconstruction of the Radon panel back into the time-space domain and the residual gather which is the difference between the full reconstructed gather from the original gather are shown in Figure 17 and Figure 18, respectively. The residual gather is only random noise and shows very minor amplitudes compared to Figure 13 and Figure 17. The success of the optimized semblance-weighted Radon method is again verified on the real data example by the two figures, Figure 17 and Figure 18.

The two primaries located at around 0q on the q-axis, and 2.2s and 2.7s in time, indicated by the pick circles, can easily be separated from the multiple reflections which are mainly on the positive side on the q-axis (Figure 16). The primaries are muted in this Radon panel, indicated by the blue curves in Figure 16, before the inverse Radon transform is performed so that only multiple reflections are reconstructed back to the time-space domain (Figure 19). The multiple-free gather is then obtained by subtracting the multiple-only gather from the original gather and the result is shown in Figure 20. We can see that the multiple-free gather is free of primaries and the primary-only gather contains only the primaries and random noise.

In order to further examine the processing results of the Radon transform, the modelled multiple gather and the primary gather are inverse NMO-corrected, as shown in Figure 21 and Figure 22, respectively and the corresponding semblance plots are shown in Figure 23 and Figure 24, respectively. Only energy from multiple reflections is left out in Figure 23 and only energy from primary reflections remains in Figure 24.

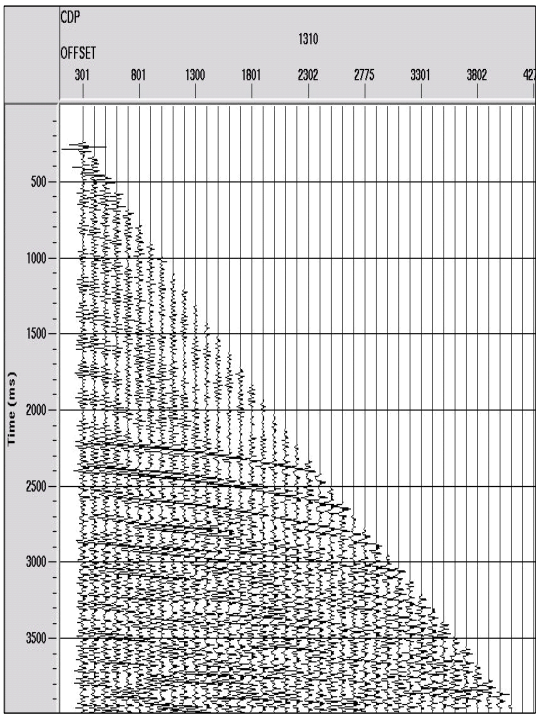

FIG. 13. The original CMP gather.

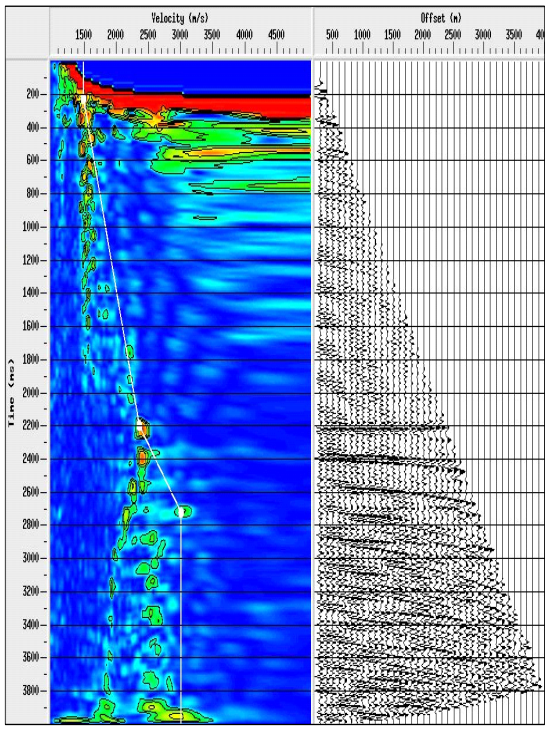

FIG. 14. The semblance plot of the CMP gather in Figure 13.

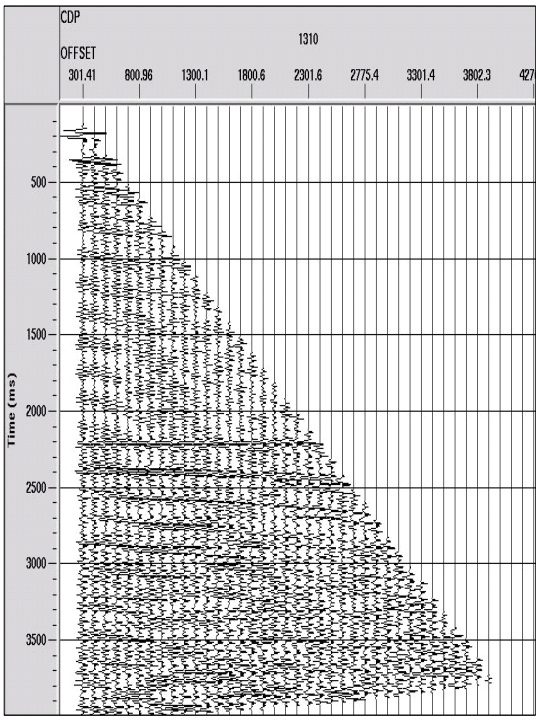

FIG. 15. The NMO-corrected CMP gather.

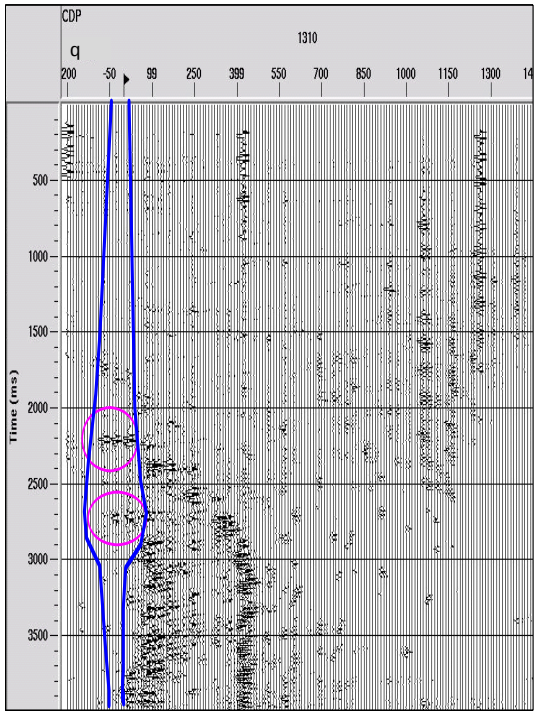

FIG. 16. The Radon panel obtained by the optimized semblance-weighted Radon transform method. Primaries are indicated by circles. The blue curves indicate the muting boundaries.

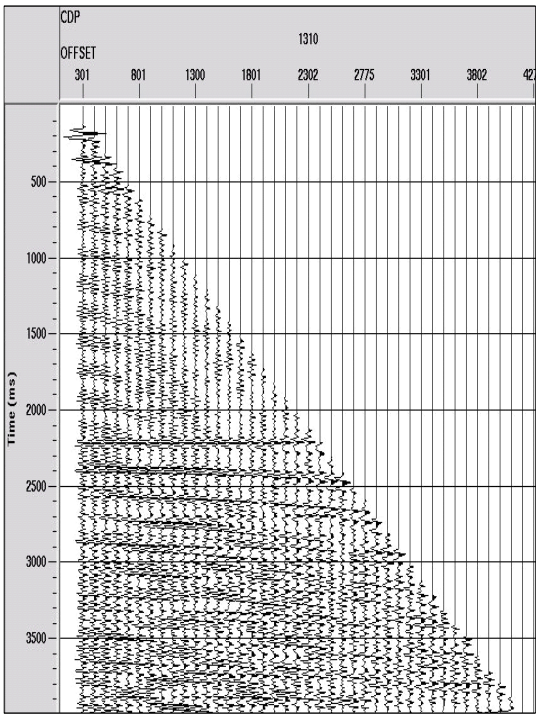

FIG. 17. The full reconstruction of the CMP gather from Figure 16. (Scaled to Figure 13)

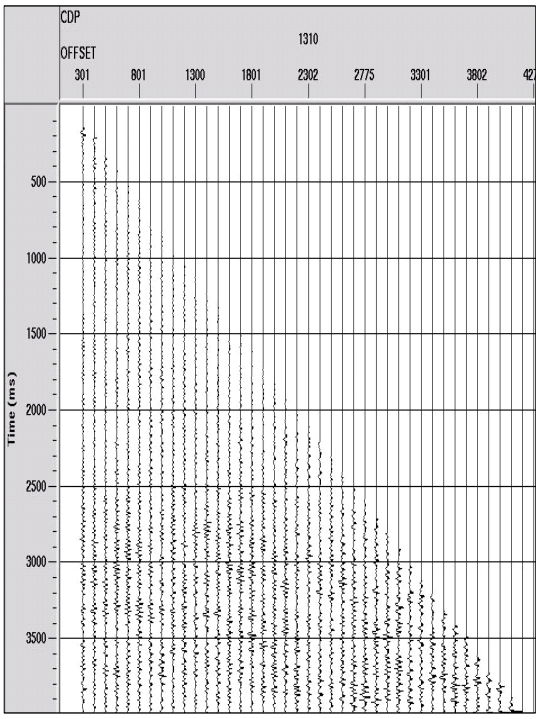

FIG. 18. The difference between the full reconstruction and the original CMP gather. (Scaled to Figure 13)

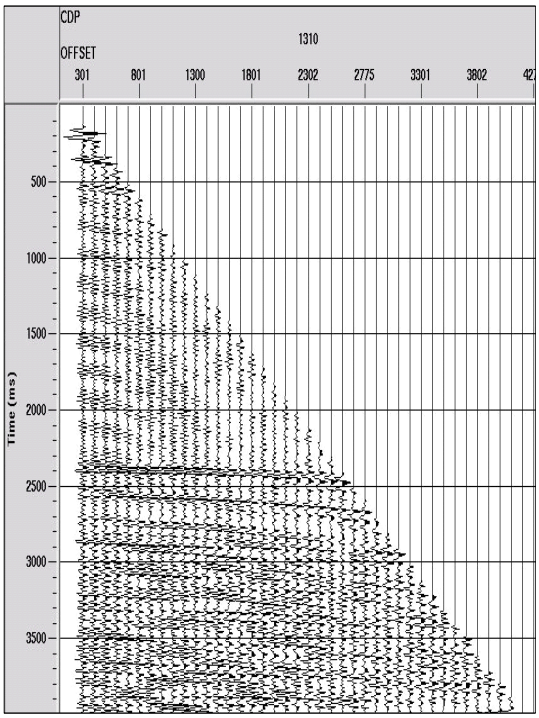

FIG. 19. The reconstructed multiple-only gather. (Scaled to Figure 13)

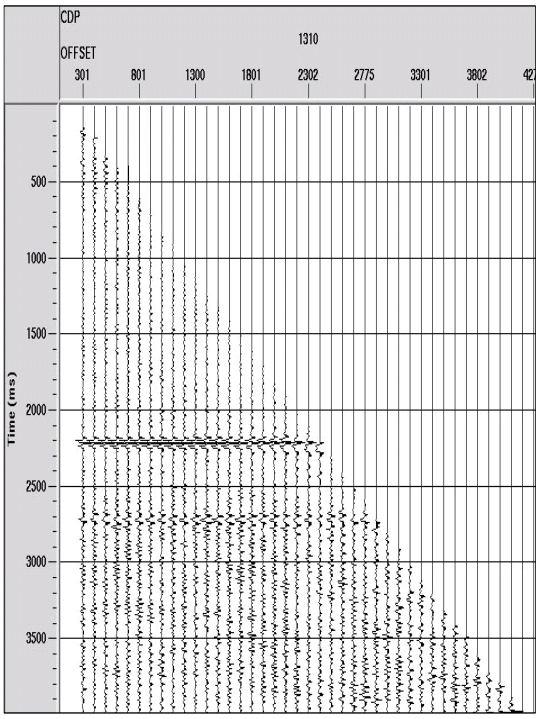

FIG. 20. The modelled primary-only gather obtained by subtracting the multiple-only gather from the original CMP gather. (Scaled to Figure 13)

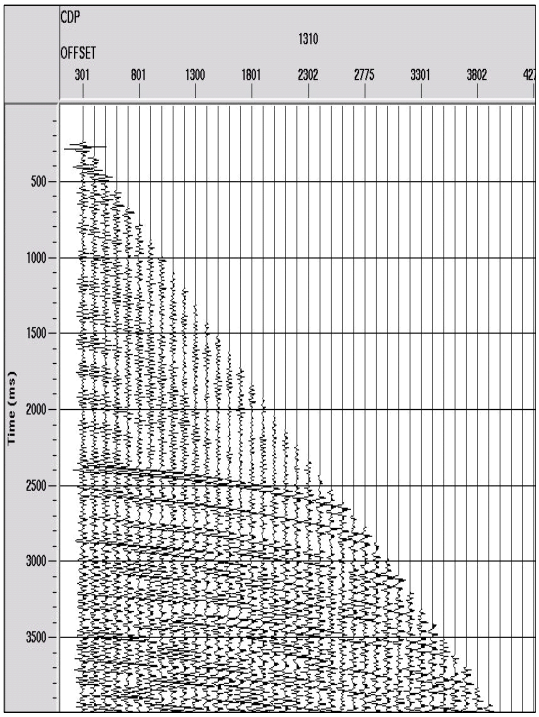

FIG. 21. The inverse NMO-corrected multiple-only gather from Figure 19. (Scaled to Figure 13)

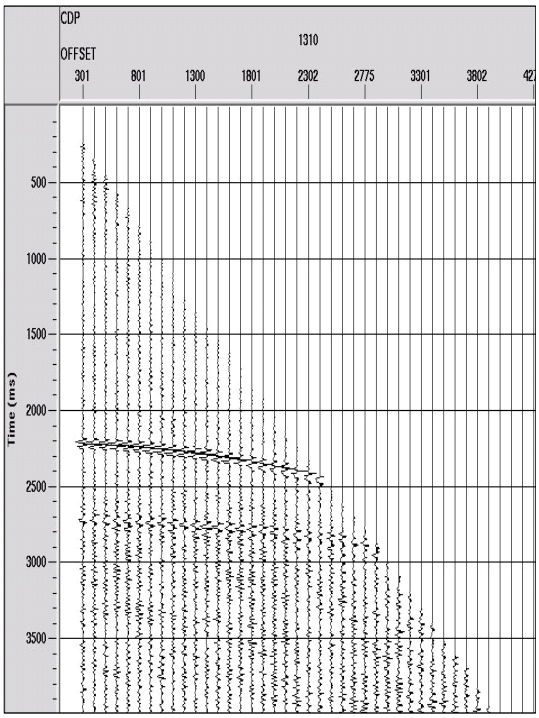

FIG. 22. The inverse NMO-corrected primary-only gather from Figure 20. (Scaled to Figure 13)

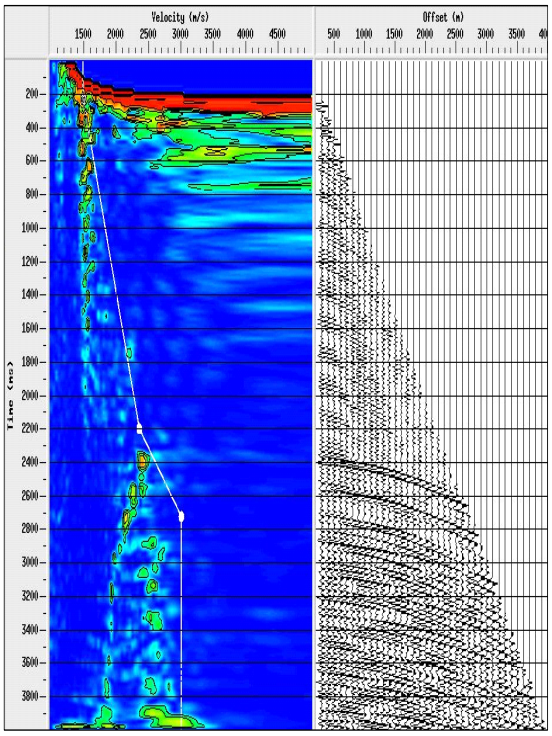

FIG. 23. The semblance plot of the modelled multiple-only gather.

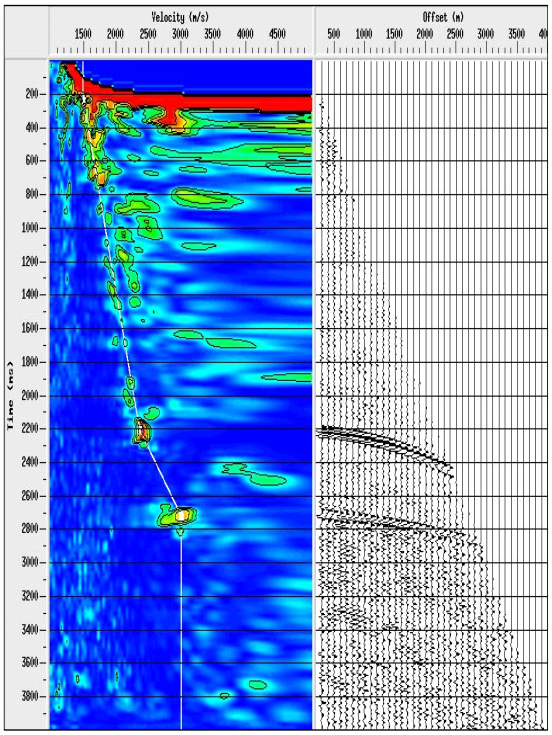

FIG. 24. The semblance plot of the modelled primary-only gather.

The conventional stack section and the section with the optimized semblance-weighted Radon technique applied are shown in Figure 25 (a) and (b), respectively. Comparing the two sections, multiples are very strong in Figure 25 (a) and reduced in (b). Some weaker primary events become visible after multiple attenuation technique is applied.

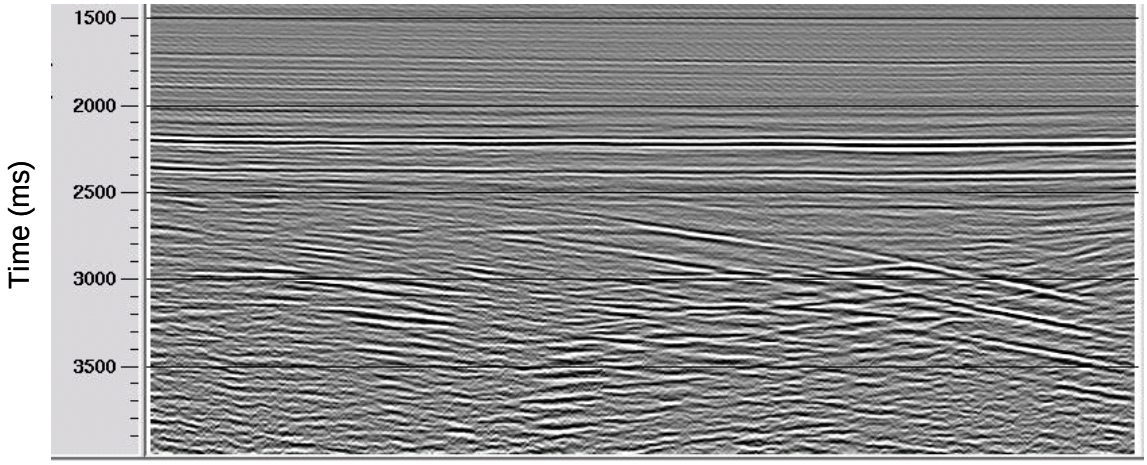

(a)

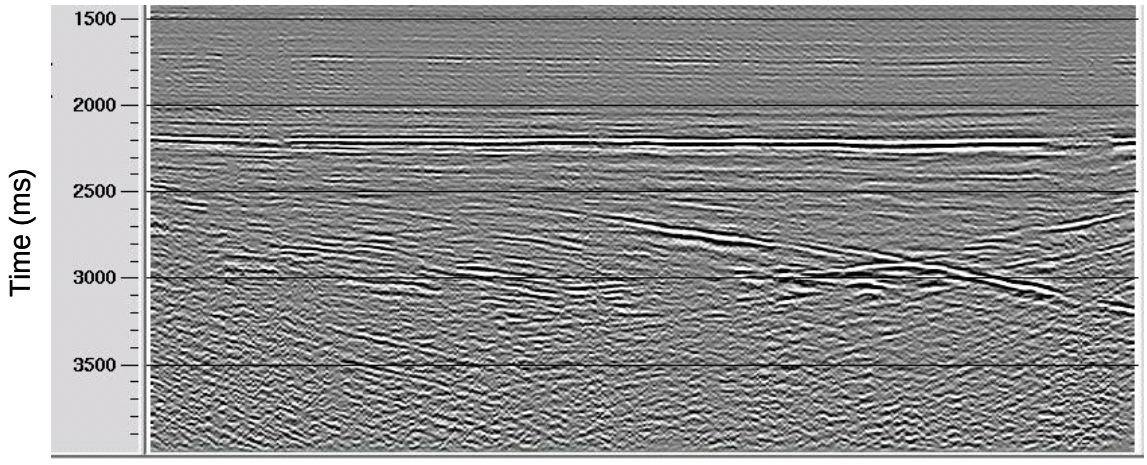

(b)

Figure 25. (a) The stack section without multiple attenuation technique applied; (b) the stack section with the optimized semblance-weighted Radon method applied on multiple attenuation.

CONCLUSIONS

The high-resolution time-domain Radon transform is an optimized solution of the semblance-weighted Radon transform. The application of the algorithm onto both the synthetic and real datasets verified its validity in the aspects of both resolution and preservation ability.

ACKNOWLEDGEMENTS

The authors acknowledge the support of CREWES sponsors and staff for this work.

REFERENCES

Bradshaw, A., and Ng, M., 1987, Multiple attenuation by parabolic stack Radon transform: Geo-X Systems internal paper.

Cao, Z., Bancroft, J. C., Brown, R. J., and Xiao, C., 2003, Radon transform and multiple attenuation: CREWES Research Report, **15**.

Cao, Z., and Bancroft, J. C., 2004, Multiple attenuation by semblance weighted Radon transform: CREWES Research Report, **16**.

Cao, Z., and Bancroft, J. C., 2005, Radon transforms and multiple attenuation of White Rose data: CREWES Research Report, **17**.

Hampson, D., 1986, Inverse velocity stacking for multiple elimination: J. Can. Soc. Expl. Geophys., **22**, 44-55.

Ng, M., and Perz, M., 2004, High resolution Radon transform in the *t-x* domain using "intelligent" prioritization of the Gauss-Seidel estimation sequence: Presented at the 74th Ann. Internat. Mtg, Soc. Expl. Geophys., Expanded Abstracts, 2160-2163.

Radon, J., 1917, Über die Bestimmung von Funktionen durch ihre Integralwerte Längs gewisser Mannigfaltigkeiten, Berichte Sächsische Akadamie der Wissenschaften, Leipzig, Math.-Phys. Kl., **69**, 262-267.

Stoffa, P. L., Buhl, P., Diebold, J. B., and Wenzel, F., 1981, Direct mapping of seismic data to the domain of intercept time and ray parameter — A plane-wave decomposition: Geophysics, **46**, 255-267.

Yilmaz, Ö., 1989, Velocity-stack processing: Geophys. Prosp., **37**, 357-382.